Equilibrium direction of magnetization under coherent rotation

Tie-Gen Song(宋铁根), Yang Hu(胡阳), De-Sheng Xue(薛德胜)

Citation: Chin. Phys. B. 35, 100204 (2026). DOI: 10.1088/1674-1056/ae23ad | CSTR: 32038.14.CPB.ae23ad
http://cpb.iphy.ac.cn; http://iopscience.iop.org/cpb

What follows is a list of articles you may be interested in

Stability switching and hopf bifurcation in a two-delay predation system with diffusion and network coupling

Wenjie Yang(杨文杰), Jingxin Hu(胡静欣), Qianqian Zheng(郑前前), Jianwei Shen(申建伟), Yiping Lin(林怡平)

Chin. Phys. B. 35, 080204 (2026). DOI: 10.1088/1674-1056/ae5c8a | CSTR: 32038.14.CPB.ae5c8a

Anti-function solution of uniaxial anisotropic Stoner-Wohlfarth model

Kun Zheng(郑坤), Yu Miao(缪宇), Tong Li(李通), Shuang-Long Yang(杨双龙), Li Xi(席力), Yang Yang(杨洋), Dun Zhao(赵敦), De-Sheng Xue(薛德胜)

Chin. Phys. B. 31, 040202 (2022). DOI: 10.1088/1674-1056/ac401e

Direct immune-SCIR public-opinion propagation model based on real-time online users

Yun-Ming Wang(王运明), Tian-Yi Guo(郭天一), Wei-Dong Li(李卫东), Bo Chen(陈波)

Chin. Phys. B. 29, 100204 (2020). DOI: 10.1088/1674-1056/aba9c0

Equilibrium direction of magnetization under coherent rotation

Tie-Gen Song(宋铁根), Yang Hu(胡阳), and De-Sheng Xue(薛德胜)†

School of Physical Science and Technology, Lanzhou University, Lanzhou 730000, China

(Received 23 September 2025; revised manuscript received 21 November 2025; accepted manuscript online 25 November 2025)

The Stoner–Wohlfarth (SW) model describes coherent rotation of magnetization with uniaxial anisotropy. However, the traditional SW model can be analytically solved only for three specific directions, making it challenging to determine the direction of equilibrium magnetization in anisotropic ferromagnets under arbitrary fields. In this study, the uniaxial anisotropy energy in the SW model is extended to include a fourth-order term. By employing inverse function theory, an exact analytical solution for the equilibrium magnetization direction under any external field is derived. The impact of the fourth-order term on hysteresis loops is analyzed, showing increased coercivity for fields parallel to the easy axis and enhanced saturation fields for perpendicular ones. These results improve the understanding of static magnetism and provide a foundation for the quantitative analysis of magnetization scattering by electric and spin currents.

Keywords: magnetization, equilibrium direction, coherent rotation, magnetic hysteresis loop

PACS: 02.60.Cb, 75.30.Gw, 75.40.Cx, 75.60.Ej

DOI: 10.1088/1674-1056/ae23ad **CSTR:** 32038.14.CPB.ae23ad

1. Introduction

The equilibrium direction of magnetization is fundamental to characterizing both the static and dynamic properties of ferromagnets,[1–4] and it plays a crucial role in describing magnetization scattering under electric and spin currents.[5,6] Since the three basic magnetization and reversal processes, namely coherent rotation,[7] displacement of domain wall,[8] and nucleation and growth,[9] may coexist, quantifying the intrinsic magnetization and anisotropy of domain-structured ferromagnets from magnetic measurements remains highly challenging.[10–12] It is known that there is exchange interaction between atomic magnetic moments, and these processes can be viewed microscopically as coherent rotation of atomic magnetic moments. Thus, quantitatively describing the coherent rotation of atomic magnetic moments or magnetization is essential for understanding the static and dynamic behavior of ferromagnetic materials.

The Stoner–Wohlfarth (SW) model, a simple framework for coherent magnetization rotation,[13] employs the simplest uniaxial anisotropy free energy $F = K_1 \sin^2(\beta - \alpha)$, where K_1 is the anisotropy constant, and β and α represent the angles between the applied magnetic field and the easy axis, and the magnetization direction, respectively. In principle, the model can determine the static equilibrium magnetization direction,[14] and subsequently predict relaxation[15] and precession.[16] As a result, the SW model is widely applied to magnetization curves and hysteresis loops for intrinsic parameter determination; it also describes dynamic behavior, characterizes frequency-dependent permeability, and investigates ferromagnetic spin electron transport,[17–19] thereby revealing the effects of magnetization, anisotropy, and interfacial spin–orbit coupling on resistance and the Hall effect.[20,21]

However, even for the equilibrium magnetization direction in the SW model, the solution requires solving a quartic equation.[22] Closed-form analytical solutions are available only when the angle between the applied magnetic field and the easy axis is 0°, 45° or 90°.[1] Thus, a precise quantitative understanding of coherent magnetization rotation remains elusive.[23]

In ferromagnets, the free energy of magnetocrystalline anisotropy inherently includes higher-order anisotropy terms, which are widely observed and strongly influence magnetization processes. For example, permanent magnetic materials with hexagonal or tetragonal structures exhibiting an easy *c*-axis can transform into easy *ab*-plane soft magnetic materials upon temperature variation,[24] which clearly indicates the significant role of higher-order terms. As the composition varies, the fourth-order constant K_2 in $Co_7Zn_7Mn_6$ and $Co_8Zn_8Mn_4$ at low temperatures is comparable to K_1 in $Co_9Zn_9Mn_2$ and even dominates in $Co_{10}Zn_{10}$.[25] In Fe/GaN(0001) epitaxial films, K_3 reaches $4.7 \sim 9.2\times10^5$ erg/cm^3 (1 erg = 10^{-7} J) and is comparable to or larger than K_1.[26] Higher-order effects are also observed in Co/Ni multilayers[27] and Fe–Pt core–shell structures.[28] These results demonstrate that a proper understanding of higher-order anisotropy terms is important for analyzing both static and dynamic magnetic properties.

This study considers an extended uniaxial anisotropy model with higher-order terms. Inspired by inverse trigonometric methods,[29] a solution is derived by inverting $y = g(x)$ to $x = f(y)$, yielding a simple analytical expression valid for general field directions. Based on the resulting equilibrium

†Corresponding author. E-mail: xueds@lzu.edu.cn

© 2026 Chinese Physical Society and IOP Publishing Ltd. All rights, including for text and data mining, AI training, and similar technologies, are reserved.

positions, angle-dependent hysteresis loops are calculated, revealing behaviors distinct from the conventional SW model. These findings provide a consistent quantitative framework for describing coherent magnetization rotation and enhance the understanding of static and dynamic magnetic properties in ferromagnets.

2. Analytical solution of the extended SW model

Consider a uniaxial anisotropic spherical particle with magnetization $\boldsymbol{M}$ deviating from the easy axis by an angle θ under an external magnetic field $\boldsymbol{H}$, as shown in Fig. 1. When the uniaxial anisotropy includes both second- and fourth-order symmetries, the free energy density of the system can be expressed as

$$F = K_1\sin^2(\beta-\alpha) + K_2\sin^4(\beta-\alpha) - \mu_0 MH\cos\alpha, \quad (1)$$

where α is the angle between $\boldsymbol{H}$ and $\boldsymbol{M}$, and β is the angle between the easy axis and $\boldsymbol{H}$. At equilibrium, $\boldsymbol{M}$ satisfies $\partial F/\partial\alpha = 0$ and $\partial^2 F/\partial\alpha^2 > 0$, which is

$$2(1+k)\sin 2(\beta-\alpha) - k\sin 4(\beta-\alpha) - 4h\sin\alpha = 0, \quad (2)$$

$$w = (1+k)\cos 2(\beta-\alpha) - k\cos 4(\beta-\alpha) + h\cos\alpha > 0, \quad (3)$$

where $k = K_2/K_1$, $h = H/H_K$, and $H_K = 2K_1/\mu_0 M$.

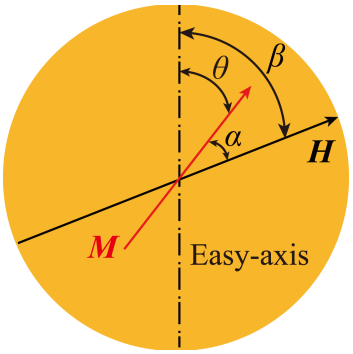

Fig. 1. Coherent rotation model of magnetization.

By defining $m = \cos\alpha$, equation (2) can be transformed into the following form:

$$4(1-m^2)\{m[(1+k)\cos 2\beta - k(2m^2-1)\cos 4\beta] + h\}^2 = [(1+k)(2m^2-1) - k(8m^4-8m^2+1)\cos 2\beta]^2\sin^2 2\beta. \quad (4)$$

From Eq. (4), it is evident that the equation is an eighth-degree one for m, which is difficult to solve analytically. However, by adopting an inverse function approach, equation (4) can be reformulated as a quadratic equation in h, leading to a straightforward analytical solution

$$h_\pm = -m\left[(1+k)\cos 2\beta - k(2m^2-1)\cos 4\beta\right] \pm \frac{(1+k)(2m^2-1) - k(8m^4-8m^2+1)\cos 2\beta}{2\sqrt{1-m^2}}\sin 2\beta. \quad (5)$$

Equation (5) thus establishes the relationship between h and m.

To determine the stable orientation of $\boldsymbol{M}$, equation (3) is employed to evaluate the stability condition $w > 0$. Following a similar method, equation (3) is treated to obtain that

$$w_\pm = (1+k)(2m^2-1)\cos 2\beta - k(8m^4-8m^2+1)\cos 4\beta + mh_\pm \pm 2m\sqrt{1-m^2}\left[(1+k) - 4k(2m^2-1)\cos 2\beta\right]\sin 2\beta. \quad (6)$$

Substituting Eq. (5) into Eq. (6) yields

$$w_\pm = (m^2-1)\left[(1+k)\cos 2\beta - k(6m^2-1)\cos 4\beta\right] \pm m\frac{(1+k)(3-2m^2) + k(24m^4-40m^2+15)\cos 2\beta}{2\sqrt{1-m^2}}\sin 2\beta. \quad (7)$$

Equation (7) therefore provides the relationship between m and β under stable conditions.

Figure 2 shows the calculated results of Eqs. (5) and (7) for $\beta = 45°$ with $k = 0$, 0.5, 1.0. It can be observed that when $m \to 1$ ($m \to -1$), $h_+ > 0$ ($h_- < 0$), $w_+ > 0$ ($w_- > 0$), indicating that h_+ and h_- correspond to w_+ and w_-, respectively. Moreover, when the direction of h changes, the solution h_+ (h_-) exhibits a discontinuous jump at the point where w_+ (w_-) equals zero. This transition identifies the stability range of solutions for different values of h.

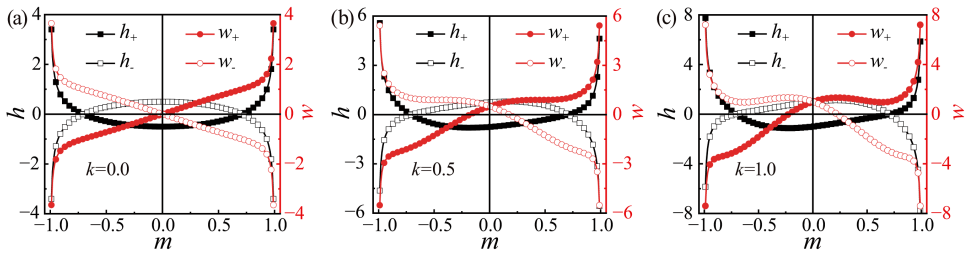

Fig. 2. Solutions of $h_\pm \sim m$ and their corresponding $w_\pm \sim m$ at $\beta = 45°$. The black solid squares correspond to $h_+ \sim m$, the black open squares correspond to $h_- \sim m$, the red solid circles correspond to $w_+ \sim m$, and the red open circles correspond to $w_- \sim m$ for (a) $k = 0$, (b) $k = 0.5$, and (c) $k = 1.0$.

Clearly, the solution of Eq. (5) is not applicable when $m^2 = 1$, *i.e.*, $\sin\alpha = 0$. In this case, the expanded form of Eq. (2) can be written as

$$\sin 2\beta\left[(1+k) - k\cos 2\beta\right] = 0. \tag{8}$$

Given that $k \leq 1$ and $0^\circ \leq \beta \leq 90^\circ$, to satisfy $1 - k\cos 2\beta \geq 0$, it is necessary that $\sin 2\beta = 0$, that is, $\beta = 0^\circ$ or 90°.

For $\beta = 0^\circ$, equations (2) and (3) reduce to

$$\left(1-m^2\right)\left\{m\left[(1+k) - k\left(2m^2-1\right)\right] + h\right\}^2 = 0, \tag{9}$$

$$w = (1+k)\left(2m^2-1\right) - k\left(8m^4-8m^2+1\right) + mh > 0. \tag{10}$$

Two types of solutions can be obtained from Eq. (9),

$$m^2 = 1, \tag{11a}$$

$$h = -m\left[(1+k) - k\left(2m^2-1\right)\right]. \tag{11b}$$

By substituting Eq. (11) into Eq. (10), the corresponding second derivatives of the free energy satisfy

$$w = 1+mh > 0, \tag{12a}$$

$$w = \left(1-m^2\right)\left(6km^2 - 2k - 1\right) > 0. \tag{12b}$$

Combining Eqs. (11) and (12), the stable solution is given by the following expressions:

$$\begin{cases} m = 1, & h > -1, \\ m\left[(1+k) - k\left(2m^2-1\right)\right] = -h, & -4km^3 < h < -1, m > 0, \\ m\left[(1+k) - k\left(2m^2-1\right)\right] = -h, & 1 < h < -4km^3, m < 0, \\ m = -1, & h < 1. \end{cases}$$

For $\beta = 90^\circ$, equations (2) and (3) reduce to

$$\left(1-m^2\right)\left\{m\left[(1+k) + k\left(2m^2-1\right)\right] - h\right\}^2 = 0, \tag{13}$$

$$w = -(1+k)\left(2m^2-1\right) - k\left(8m^4-8m^2+1\right) + mh > 0. \tag{14}$$

From Eq. (13), two types of solutions are also obtained

$$m^2 = 1, \tag{15a}$$

$$h = m\left[(1+k) + k\left(2m^2-1\right)\right]. \tag{15b}$$

Substituting Eq. (16) into Eq. (14) yields the corresponding second derivatives of the free energy

$$w = -1 - 2k + mh > 0, \tag{16a}$$

$$w = \left(1-m^2\right)\left(1+6km^2\right) > 0. \tag{16b}$$

Combining Eqs. (16) and (17), the stable solutions are

$$\begin{cases} m = 1, \\ h = m\left[(1+k) + k\left(2m^2-1\right)\right], \\ m = -1, \end{cases} \quad \begin{array}{l} h \geq (1+2k), \\ -(1+2k) < h < (1+2k), \\ h \leq -(1+2k). \end{array}$$

3. Static hysteresis loops

Using Eqs. (13) and (17), the hysteresis loops for $\beta = 0^\circ$ and 90° can be calculated.

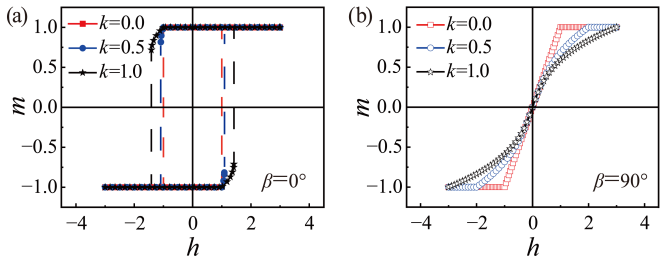

Fig. 3. Magnetic hysteresis loops for different k values. The red squares correspond to $k = 0$, the blue circles correspond to $k = 0.5$, and the black asterisks correspond to $k = 1.0$. Solid symbols correspond to $\beta = 0^\circ$, and open symbols correspond to $\beta = 90^\circ$. The symbols represent stable solutions, and the dashed lines represent jump points for (a) $\beta = 0^\circ$ and (b) $\beta = 90^\circ$.

Figure 3 shows the corresponding hysteresis loops for $\beta = 0^\circ$ and 90° with $k = 0.0$, 0.5, and 1.0. It can be observed that the hysteresis loop at $\beta = 0^\circ$ is independent of k, while the loop at $\beta = 90^\circ$ exhibits significant variation with increasing k. Two main features are observed: first, the central part of the loop evolves from a straight line to an S-shaped curve; second, the saturation field becomes larger than that at $\beta = 0^\circ$. These two features can be used to distinguish whether the anisotropy of the system conforms to the assumptions of the SW model.

Generally, the hysteresis loop can be determined by jointly using Eqs. (5) and (7). Following the typical procedure for measuring hysteresis loops, h starts at a large positive value, where $w_+ > 0$ and $w_- < 0$, indicating that the solution of $h_+ \sim m$ represents the physically stable solution. As h_+ gradually decreases, once it crosses the point where $w_+ = 0$, a transition occurs such that $w_+ < 0$ and $w_- > 0$. At this stage, $h_- \sim m$ becomes the appropriate stable solution, and remains so until the system reaches magnetic saturation. Conversely, when h increases from a large negative value, $w_- > 0$ indicates that $h_- \sim m$ corresponds to the stable solution. Once the

system crosses the point where $w_- = 0$, the condition switches to $w_+ > 0$ and $w_- < 0$, in which case $h_+ \sim m$ becomes the valid solution. Based on the above procedure, hysteresis loops under various conditions can be obtained. Figure 4 shows the hysteresis loops for $\beta = 22.5°$, $45°$, and $77.5°$ with $k = 0$, 0.5, and 1.0.

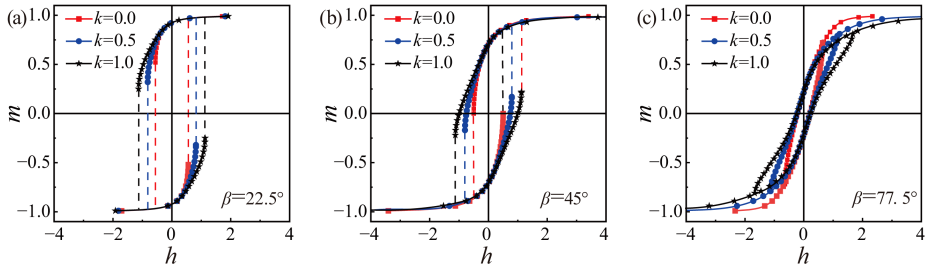

Fig. 4. Magnetic hysteresis loops for $k = 0$, 0.5, and 1.0. The red solid squares correspond to $k = 0.0$, the blue solid circles correspond to $k = 0.5$, and the black solid asterisks correspond to $k = 1.0$ for (a) $\beta = 22.5°$, (b) $\beta = 45°$, and (c) $\beta = 77.5°$.

4. Discussion

Based on the hysteresis loop solutions, the dependence of remanence m_r, saturation field h_s, switching field h_{SF}, and coercivity h_c on β is extracted, as shown in Fig. 5. The remanence corresponds to the point $(h = 0, m_r)$ and can be obtained from Eq. (2) as

$$m_r = \cos\alpha = \cos\beta. \tag{17}$$

As shown in Fig. 5(a), m_r is independent of k and depends solely on the direction of h.

The saturation field h_s corresponds to the point $(h_s, m = 1)$. However, true saturation is unattainable for field directions other than $\beta = 0°$ and $90°$. The value of h_s can be obtained using Eq. (5)

$$h_s = -m\left[(1+k)\cos 2\beta - k\left(2m^2-1\right)\cos 4\beta\right] + \frac{(1+k)\left(2m^2-1\right) - k\left(8m^4-8m^2+1\right)\cos 2\beta}{2\sqrt{1-m^2}}\sin 2\beta. \tag{18}$$

Assuming that $m = 0.99$ corresponds to a near-saturated state, h_s for different magnetization directions can be determined accordingly, as shown in Fig. 5(b). It is evident that h_s varies significantly with different easy-axis orientations. Moreover, h_s increases progressively with increasing k.

It is known that h_{SF} can be determined by simultaneously setting $h_\pm = w_\pm = 0$ in Eqs. (5) and (6). Although h_{SF} has an analytical expression in the conventional SW model, it becomes difficult to obtain a closed-form solution when the fourth-order anisotropy term is included. To address this, we set $w_\pm = 0$ in Eq. (7) and compute the values of m for different β. Substituting these values back into Eq. (6), h_{SF} can be obtained. As shown in Fig. 5(c), all switching fields are represented by star-shaped curves, which expand outward with increasing k.

The existence of the switching field also leads to two distinct types of coercivity solutions. The first solution corresponds to $m > 0$, consistent with switching fields, while the second corresponds to $m = 0$, which can be derived from Eq. (5) as

$$h_c = -\frac{1}{2}\left(1+2k\cos^2\beta\right)\sin 2\beta. \tag{19}$$

As shown in Fig. 5(d), the coercivity gradually decreases with increasing β, and generally increases with larger values of k.

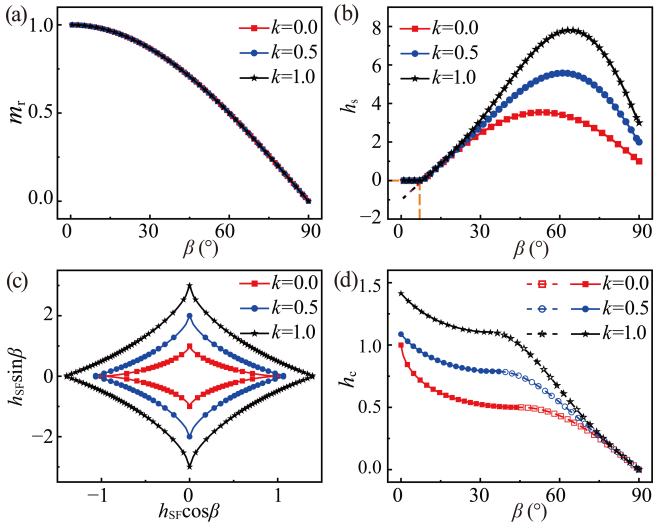

Fig. 5. Variation of characteristic quantities with β for $k = 0$, 0.5, and 1.0. The red solid squares correspond to $k = 0.0$, the blue solid circles correspond to $k = 0.5$, and the black solid asterisks correspond to $k = 1.0$, for (a) remanence m_r, (b) saturation field h_s. The dashed line represents the results of theoretical calculations using Eq. (18), and the solid line indicates the results of actual measurements. (c) Switching field h_{SF}. (d) Coercivity h_c. The solid line is obtained from h_{SF}, and the dashed line is derived from Eq. (19).

5. Conclusion

In this study, an analytical solution to the extended SW model is derived, and the static magnetic behavior of magnetization along arbitrary directions is investigated. Using the inverse function concept, the exact analytical solution for the equilibrium direction of magnetization is obtained in a general uniaxial anisotropic system under arbitrary field directions. Based on this stable solution, hysteresis loops under arbitrary field directions are obtained, which show distinct differences

from conventional expectations. The analytical solution establishes criteria and characteristics for understanding static magnetization under the coherent rotation mechanism. From the single-domain particle perspective, increasing k alongside reducing β is an effective approach to enhance coercivity for hard magnetic particles. In contrast, for soft magnetic materials, reducing anisotropy and adjusting the magnetization direction is the most effective approach to minimizing losses. This work provides an exact analytical framework for the extended SW model under arbitrary field orientations, which can be used to investigate the effect of higher-order terms on the dynamic magnetization processes.

Acknowledgements

Project supported by the National Key Research and Development Program of China (Grant No. 2021YFB3501300), the National Natural Science Foundation of China (Grant No. 12174163), and the 111 Project (Grant No. B20063).

References

[1] Stoner E C and Wohlfarth E P 1991 *IEEE Trans. Magn.* **27** 3475
[2] Wang Z Y and Sun Z Z 2014 *J. Appl. Phys.* **115** 063905
[3] Belashchenko K D 2010 *Phys. Rev. Lett.* **105** 147204
[4] Neeraj K, Awari N, Kovalev S, Polley D, Hagström N Z, Arekapudi S S P K, Semisalova A, Lenz K, Green B, Deinert J C, Ilyakov I, Chen M, Bawatna M, Scalera V, d'Aquino M, Serpico C, Hellwig O, Wegrowe J E, Gensch M and Bonetti S 2021 *Nat. Phys.* **17** 245
[5] Wang R X, Ye H, Wang L J and Ao Z H 2017 *Acta Phys. Sin.* **66** 127201 (in Chinese)
[6] Inoue J and Brataas A 2004 *Phys. Rev. B* **70** 140406
[7] Zhong W D 2017 *Ferromagnetism*, 2nd edn. (Beijing: Science Press) pp. 142–145
[8] Jiles D C and Atherton D L 1986 *J. Magn. Magn. Mater.* **61** 48
[9] Kronmuller H, Durst K D and Sagawa M 1988 *J. Magn. Magn. Mater.* **74** 291
[10] Marioni M A, Pilet N, Ashworth T V, O'Handley R C and Hug H J 2006 *Phys. Rev. Lett.* **97** 027201
[11] Zhuravlev V A and Oshlakov A A 2001 *Phys. Solid State* **43** 2110
[12] Alves T M L, Bezerra C G, Viegas A D C, Nicolodi S, Corrêa M A and Bohn F 2015 *J. Appl. Phys.* **117** 083901
[13] Sui W B, Zhu J Y, Li J Y, Chai G Z, Jiang C J, Fan X L and Xue D S 2011 *J. Appl. Phys.* **109** 103902
[14] Stancu A and Chiorescu I 1997 *IEEE Trans. Magn.* **33** 2573
[15] Zhang Z N, Jia Z L and Xue D S 2024 *Chin. Phys. B* **33** 047502
[16] Becker J, Mosendz O, Weller D, Kirilyuk A, Maan J C, Christianen P C M, Rasing T and Kimel A 2014 *Appl. Phys. Lett.* **104** 152412
[17] Miao Y, Yang D Z, Jia L, Li X L, Yang S L, Gao C X and Xue D S 2021 *Appl. Phys. Lett.* **118** 042404
[18] Yan S, Sun Z L and Bazaliy Y B 2013 *Phys. Rev. B* **88** 054408
[19] Wang X R and Sun Z Z 2008 *J. Appl. Phys.* **103** 07D901
[20] Li S F and Zhu T 2020 *Jpn. J. Appl. Phys.* **59** 040906
[21] Shi G Y, Wan C H, Chang Y S, Li F, Zhou X J, Zhang P X, Cai J W, Han X F, Pan F and Song C 2017 *Phys. Rev. B* **95** 104435
[22] Wood R 2009 *IEEE Trans. Magn.* **45** 100
[23] Xue D and Ma W G 2019 *Electronics* **8** 366
[24] Otani Y, Hurley D P F, Sun H and Coey J M D 1991 *J. Appl. Phys.* **69** 5584
[25] Preißinger M, Karube K, Ehlers D, Szigeti B, Nidda H A K V, White J S, Ukleev V, Rønnow H M, Tokunaga Y, Kikkawa A, Tokura Y, Taguchi Y and Kézsmárki I 2021 *Npj Quantum Mater.* **6** 65
[26] Gao C X, Dong C H, Jia C L, Herfort J, Brandt O and Xue D S 2015 *Phys. Rev. B* **92** 094404
[27] Rai A, Sapkota A, Pokhrel A, Li M, De Graef M, Mewes C, Sokalski V and Mewes T 2020 *Phys. Rev. B* **102** 174421
[28] Binh N T, Jenkins S, Ruta S, Evans R F L and Chantrell R W 2023 *Phys. Rev. B* **107** L041410
[29] Zheng K, Miao Y, Li T, Yang S L, Xi L, Yang Y, Zhao D and Xue D S 2022 *Chin. Phys. B* **31** 040202